Characterization of nanoscale property variations in polymer composite systems: Part 2 - Numerical Modeling

T. A. Bogetti†, T. Wang‡, M. R. VanLandingham‡ and J. W. Gillespie, Jr.‡
† United States Army Research Laboratory, USA
‡ Center for Composite Materials, University of Delaware

ABSTRACT

In Part 1 of the companion paper, a technique utilizing the indenting capabilities of the atomic force microscope (AFM) was used to evaluate the local changes in material response of polymer composite systems near the fiber-matrix interface. Responses for two model composite systems at both room temperature and elevated temperatures were studied. In Part 2, we compare the AFM indentation results to finite element model predictions to gain a fundamental understanding of the influence that the interphase properties have on the measured responses. Good agreement between the finite element model predictions and the AFM measured results was found for all cases studied. The finite element results confirmed that the interphase region for an unsized graphite fiber is too small (relative to the physical size of the indentation probe) to conduct realistic characterization. It was shown, however, that the sized fiber case has an interphase region sufficiently large to obtain useful measurements. The finite element model was then used to identify the effects of interphase region size on the potential usefulness of AFM indentation as a viable interphase characterization method.

Key words: *polymer composite materials; indentation; atomic force microscope; fiber-matrix interface; interphase regions; finite element analysis; epoxy resin*

INTRODUCTION

The fiber-matrix interphase plays a critical role in the behavior and performance of fiber-reinforced composite systems. A great deal of effort has been put forth conducting analytical and numerical modeling studies of the hygrothermo-mechanical behavior of interphase phenomena [1-5]. The majority of these studies can be categorized into either of two areas: (1) interphase effects on the development of micro-level residual stress and strain states or (2) relating microstructural details of the interphase can be related to the macroscopic performance characteristics of the composite material system. In all interphase modeling efforts, reliable property input is critical to accurate model predictions. The primary motivation for this work is therefore to add confidence to the interpretation of experimental findings discussed in Part 1 and help to more accurately define property gradients in interphase regions. In addition, the interphase models presented here are used to gain insight into the usefulness and limitations of AFM indentation as a viable and accurate direct interphase characterization method.

Recently, researchers have made some unique discoveries concerning the development of property gradients near the fiber-matrix interface [6-10]. In these studies, thermodynamic and kinetic models have been used to predict gradients in the amine distribution caused by the presence of the fiber surface. The predicted concentration gradients were linked to property gradients through theoretical relationships between stoichiometry and properties of the epoxy matrix. Using properties measured for unreinforced epoxy samples of different epoxy-amine ratios, the

stoichiometry profiles predicted were mapped point by point into interphase property gradients (modulus and glass transition temperature, T_g). The interphase characteristics predicted by this method were significantly different from previous models in terms of both the property gradient profiles and the absolute size of the interphase. For example, the thickness of the interphase of an unsized fiber was found to be extremely small, less than 0.1% of the fiber radius, which is nearly an order of magnitude smaller than what was previously assumed.

In this work, a unique finite element model is developed which incorporates the interphase property gradients determined by McCullough, et al. [6-10]. The model predictions of the AFM indentation response in the interphase of an unsized carbon fiber and a sized copper fiber are compared with the experimental findings of Part 1. Both room-temperature and elevated-temperature conditions are investigated. In the Analysis section, the numerical model details are presented. Property input as well as model boundary conditions are discussed. In the Results and Discussion section, model convergence characteristics and direct correlation between model predictions and measured results are presented and discussed. The significance of the results with respect to the confirmation of realistic property gradients in the interphase and the viability of AFM indentation as an accurate and direct interphase characterization method are also discussed.

ANALYSIS

Model Configurations

Two interphase case studies are investigated, an unsized carbon fiber and an epoxy-coated (or sized) copper fiber. The physical model of the unsized carbon fiber is represented with a three-phase concentric cylinder configuration as shown in Figure 1a. The fiber is an unsized AS4 fiber and the matrix is an epoxy with a 28 pph (parts per hundred) PACM 20/Epon 828 stoichiometric mixture. The indicated fiber and matrix regions are assumed to possess uniform properties. The carbon fiber is assumed to be transversely isotropic, while the matrix and interphase regions are assumed to be isotropic. The property gradients employed in the interphase region are described in the following subsection.

The physical model of the coated copper fiber is represented with the five-phase concentric cylinder configuration shown in Figure 1b. The same epoxy matrix is used, and the coating is an Epon 1001F epoxy. The indicated fiber, coating, and matrix regions are assumed to possess uniform properties. All the indicated regions are assumed to be isotropic. The property gradients employed in the first and second interphase region are described in the following section.

The constant linear-elastic material properties used in the finite element analysis are summarized in Table 1 for both model configurations. The radial thickness of the interphase used in the unsized carbon fiber configuration is 3 nm. The radial thicknesses of the first and second interphases in the coated copper fiber configuration are 3 and 1500 nm, respectively. The coating thickness on the copper fiber is 8000 nm.

Interphase Property Gradients

The relationships between amine content (measured in pph) and the epoxy modulus and glass transition temperature (T_g) are presented in Figure 2 for the epoxy system considered in this investigation [6,7]. The amine gradient in the unsized carbon fiber interphase has also been found to vary according to that indicated in Figure 3 [9,10]. A direct mapping of the modulus and T_g dependence on amine content onto the actual amine gradient profile gives the property gradients for modulus and T_g in the unsized carbon fiber interphase region as shown in Figure 4. These are the actual property values used in the finite element model for the unsized carbon fiber configuration.

Property gradients in the first interphase region of the coated copper fiber configuration are assumed identical to those in the unsized carbon fiber configuration [9]. The second interphase between the coating and matrix is much thicker. A linear gradient of amine content is assumed between the coating material (Epon 1001F) and the bulk matrix material (Epon 828), which is based on the results of the diffusion-reaction kinetics model presented in Figure 11 of the companion paper. This amine gradient is plotted in Figure 5, and the corresponding modulus and T_g gradients are shown in Figure 6.

Effects of Glass Transition and Elevated Temperatures

At temperatures above the T_g, the matrix material changes from a glassy solid to a rubbery, viscoelastic material. In our treatment of T_g gradients and elevated temperature effects, the modulus profiles within the interphase are subject to modification to reflect this softening behavior. Specifically, for regions within the model where the elevated

temperature exceeds the local T_g, the modulus is arbitrary reduced by 80% of the room-temperature value to simulate the loss of material stiffness at elevated temperatures.

Finite Element Models

Finite element representations of the physical models (See Figure 1) incorporating the interphase property gradients were constructed. The physical nature of the indentation experiment lacks convenient symmetry which might otherwise permit the used of two-dimensional axisymmetric elements. A fully three-dimensional model is therefore used to simulate the indentation experiment. Finite element models are generated with PATRAN [11], and the numerical solver employed is ABAQUS [12]. The element used in this analysis is an 8-noded three-dimensional solid element designated C3D8 in the ABAQUS manual. The number of elements needed to yield converged solutions for the interphase finite element models presented in this study typically ranged between 5000 and 10000.

A representative finite element mesh of the indentation experiment is shown in Figure 7 for the coated copper fiber configuration. Note that half-space symmetry is used to reduce the total number of elements in the model. The indentation experiment is simulated by successively applying a single unit point load (P) in the axial direction (see Figure 7) to each node along the representative surface line (AB in Figure 7) of the model and monitoring the resulting nodal deflections. Note that mesh densities are increased in the interphase regions and along the line of point load application (AB), where material gradients are defined and large stress gradients are expected.

The global model boundary conditions used are as follows: (1) the displacements perpendicular to the half-plane of symmetry are constrained in the circumferential

direction ($\delta y=0$, see Figure 7); (2) the axial z-direction displacements are constrained ($\delta z=0$) on the bottom portion of the model; and (3) the radial x-direction displacement is constrained ($\delta x=0$) at the bottom of the fiber center (point O in Figure 7).

Property gradients within the interphase regions are conveniently defined in the ABAQUS code through the use of a user-defined UMAT FORTRAN subroutine. Within the UMAT subroutine, the spatial position of each integration point is uniquely defined according to the property gradients defined in the previous sections. At elevated temperatures, the modulus reduction procedure described previously was enforced in portions of the model where temperatures exceed the local T_g of the material.

RESULTS AND DISCUSSION

Data Reduction

Results from the indentation experiments and finite element model predictions are presented in terms of a normalized stiffness. Basically, the stiffness at a point is calculated as the applied load divided by the nodal deflection. This stiffness is then normalized by a stiffness calculated for the exact same finite element model and node except with uniform bulk matrix properties assigned to the entire model. Following this procedure, normalized stiffnesses will approach unity far removed from the fiber.

Convergence Study

Application of the point load at a node requires special consideration, since the exact elastic solution for the deflection is infinite. The approach of using a distributed load on the element surface was attempted but not successful due to mesh sensitivity effects on the predicted deflections. Because of the singularity at the point load, a special

normalization method was developed. This normalization method, described below, was useful in eliminating mesh sensitivity effects from the finite element predictions.

In elasticity theory [13], the displacement at a concentrated load on a half space is given by

$$d = \frac{P(1-\nu^2)}{\pi E r} \tag{1}$$

where d is the displacement, P is the concentration load, E is the modulus of the material, υ is the Poisson's ratio, and r is the radius of the circle to which the concentrated load is applied, (r=0 is a point load). Note that as the radius tends to zero, the displacement tends to infinity.

The ratio of the displacements of two different materials with the same concentrated load (and the same Poisson's ratio) has a finite value equal to the inverse ratio of their respective moduli, as shown in the following expression:

$$\frac{d_1}{d_2} = \frac{\dfrac{P(1-\nu^2)}{\pi E_1 r}}{\dfrac{P(1-\nu^2)}{\pi E_2 r}} = \frac{E_2}{E1} \tag{2}$$

Using models with uniform mesh densities and uniform properties the relationship between element size and nodal displacement at the point load was studied. The following simple relationship between element size, L_e, and node displacement, $\bar{d}$, for a unit point load is assumed:

$$\bar{d} = \frac{AP}{EL_e} \tag{3}$$

where *P* is the concentrated load, E is the modulus of the material, and A is an arbitrary constant. Equation 3 was fit to the finite element results for five different element sizes

and two different materials. As can be seen in Figure 8, Equation 3 is shown to be an excellent fit for the finite element results. Accordingly, the ratio of displacements of two different materials (same mesh density and applied unit load) can be expressed as

$$\frac{\overline{d_1}}{\overline{d_2}} = \frac{\frac{AP}{E_1 L_e}}{\frac{AP}{E_2 L_e}} = \frac{E_2}{E1} \tag{4}$$

Comparing Equations 2 and 4, we can write

$$\frac{\overline{d_1}}{\overline{d_2}} = \frac{d_1}{d_2} \tag{5}$$

Thus, the ratio of the finite element displacements will converge to the same ratio as that based on the elasticity solution. Further, from Equations 4 and 5, the ratio of finite element displacements will converge to the inverse of the respective material moduli:

$$\frac{\overline{d_1}}{\overline{d_2}} = \frac{E_2}{E_1} \tag{6}$$

Note also that Equation 6 holds true only if the same mesh and applied load are used for each displacement calculation.

This result is important in that it justifies the stiffness normalization procedure. For each mesh, the nodal displacement calculation is made twice; (1) using constant bulk matrix material properties everywhere within the finite element model; and (2) using fiber and matrix properties along with interphase property gradients.

A mesh convergence study was conducted to verify that sufficient mesh density is obtained for reliable normalized stiffness profile calculations. The unsized carbon fiber interphase configuration at room temperature was modeled using meshes with 5000, 10000, and 15000 elements. The results are shown in Figure 9 and show sufficient mesh

density even at 5000 elements. It is noted that the coated copper fiber interphase configuration required significantly more elements (nearly 10000).

Unsized Carbon Fiber Model Results

Predicted finite element normalized stiffness profiles for the unsized carbon fiber interphase configuration at 20°C, 80°C, and 120°C are shown in Figure 10.
The increased softening effect on the normalized stiffness with increasing elevated temperature is shown. For all temperatures, the normalized stiffness approaches unity at 0.004 μm (slightly larger than the interphase size of 0.003 μm). The significance of this result is that the AFM indentor is larger than the region affected by the interphase property gradients and therefore is not capable of characterization in such a small interphase region. The normalized stiffness profile for 20°C can be compared with actual AFM measurements shown in Figure 3 of the companion paper. The AFM measurements, however, can be measured only at distances far removed from the fiber surface (e.g., 0.05 μm).

Coated Copper Fiber Model Results

Predicted finite element normalized stiffness profiles for the coated copper fiber interphase configuration at 20°C, 80°C, and 120°C are shown in Figures 11, 12, and 13, respectively. In each figure, the associated AFM indentation responses are plotted for comparison. The qualitative agreement between the radial locations of normalized stiffness changes of the respective temperature conditions supports our assumptions made about the interphase gradients.

Reasonably good agreement is seen for each temperature condition except in the region of the second interphase, where the finite element models predict a more compliant indentation response than the AFM results. Quantitative agreement in this region is not necessarily expected due to complex material and geometric interactions between the indentor and the interphase material as its T_g is approached. In addition, the actual modulus reduction profile will not be discontinuous as the finite element profile was assumed.

Note also that the significantly greater thicknesses of the second interphase region (compared with the first interphase region) enable AFM indentation to be useful as an interphase characterization method.

Interphase Size Effects on Measurable Indentation Response

The unsized carbon fiber interphase region (0.003 μm thick) proved to be too small for AFM characterization. The lateral resolution of the AFM indentor is approximately 0.05 μm and consequently, a much larger interphase region would have to exist for modulus profile characterization to be conducted. Parametric studies were performed to investigate the effects of interphase thickness on indentation response measurements. Interphase thicknesses of 0.004 μm, 0.1 μm, and 0.2 μm were investigated, and the corresponding normalized stiffness profiles are shown in Figure 14. The modulus gradient profiles for these cases were generated assuming values proportional to the unsized carbon fiber interphase configuration. Indentation response predictions for these cases were also conducted at an elevated temperature condition of 120°C, shown in Figure 15.

The results demonstrate that while the AFM is not useful for characterization of extremely small interphases, it is useful for characterization of interphase regions within its measuring sensitivity (0.05 μm). The carbon/epoxy system studied in this work might exhibit a small interphase size as compared with other fiber/matrix systems. Consequently, the AFM has the potential to be used to characterize other systems with thicker interphases.

CONCLUSIONS

Three-dimensional finite element models of an unsized carbon fiber/epoxy system and a coated copper fiber/epoxy system were constructed. Realistic interphase property gradients were employed in the models, and indentation response predictions were compared with actual AFM indentation measurements to gain a fundamental understanding of the influence the interphase properties have on the measured responses. The effects of T_g and elevated temperature were included in the study. Good agreement between the finite element model predictions and the AFM measured results were found for all cases studied. The finite element results confirmed that the interphase region in the unsized fiber is too small (as compared to the physical size of the indentation probe) to conduct realistic characterization. However, the sized fiber case involves an interphase region sufficiently large to obtain useful measurements. The finite element model was further used to identify the effects of interphase region size on the potential usefulness of AFM indentation as a viable interphase characterization method.

ACKNOWLEDGMENTS

The authors are grateful for the financial support of the U. S. Army Research Laboratory (ARL) under the Composite Materials Research Collaborative Program (CMRCP), ARL agreement number DAAL01-96-2-0048.

REFERENCES

[1] Gardner, S. D., Pittman, C. U. Jr., Hackett, R. M., Residual thermal stresses in filamentary polymer-matrix composites containing an elastomeric interphase*, J. Comp. Mat.*, 1993, **27**, pp. 830-860.

[2] Dasgupta A. and Bhandarkar S. M., A generalized self-consistent Mori-Tanaka scheme for fiber-composites with multiple interphases. *Mechanics of Materials*, **11**, 1992, pp. 7-12.

[3] Jayaraman, K., Gao Z. and Reifsnider K. L., Stress fields in continuous fiber composites with interfacial property gradients, *Proceeding from the American Society of Composites Sixth Technical Conference*, Technomic Publishing Company, Lancaster, PA, 1992, p. 759.

[4] Jayaraman, K., Reifsnider K. L., and Swain, R. E., Elastic and thermal effects in the interphase: part I. Comments on characterization methods, *J. Comp. Tech. & Res.* , 1993, **15**, pp. 3-13.

[5] Jayaraman, K., Reifsnider K. L., and Swain, R. E., Elastic and thermal effects in the interphase: part II. Comments on modeling studies, *J. Comp. Tech. & Res.* , 1993, **15**, pp. 14-22.

[6] Palmese, G. R. and McCullough, R. L., Effect of epoxy-amine stoichiometry on cured resin material properties, *J. Appl. Polym. Sci.*, 1992, **16**, pp. 1163-1173.

[7] Palmese, G. R. and McCullough, R. L., Kinetic and thermodynamic considerations regarding interphase formation in thermosetting composite systems, *J. Adhesion*, 1991, **11**, pp. 19-29.

[8] Palmese, G. R., Origin and influence of interphase material property gradients in thermosetting composites, Ph.D. Thesis, Chemical Engineering Department, University of Delaware, 1992.

[9] Skourlis, T. P. and McCullough R. L., The effect of temperature on the behavior of the interphase on polymeric composites, *Comp. Sci. and Tech.*, 1993., **19**, pp. 363-361.

[10] Skourlis T. P., Structure and properties of the interphase in coated carbon-fiber/Epoxy systems, Ph.D. Thesis, Chemical Engineering Department, University of Delaware. 1996.

[11] PDA Engineering, PATRAN Division, *PATRAN Plus User Manual*, Release 5.0, Costa Mesa, CA: Author, 1997.

[12] Hibbitt, Karlsson and Sorensen, Inc., *ABAQUS User's Manual*, Version 5.4, Pawtucket, RI: Author, 1996.

[13] Timoshenko, S.P. and Goodier, J.N., *Theory of Elasticity*, New York, McGraw-Hill Book Company, Inc., 1970, p. 402.

LIST OF TABLES

LIST OF FIGURES

Table 1. Uniform fiber and matrix properties

AS4 Fiber		Copper Fiber	Coating	Bulk Matrix
E_{11}=241 Gpa E_{22}=21 Gpa E_{33}=21 Gpa G_{12}=96.4 Gpa G_{13}=96.4 Gpa G_{23}=8.4 Gpa	ν_{12}=0.25 ν_{23}=0.25 ν_{13}=0.25	E=120 Gpa ν=0.25	E=3.1 Gpa ν=0.35	E=2.3 Gpa ν=0.35 T_g=160

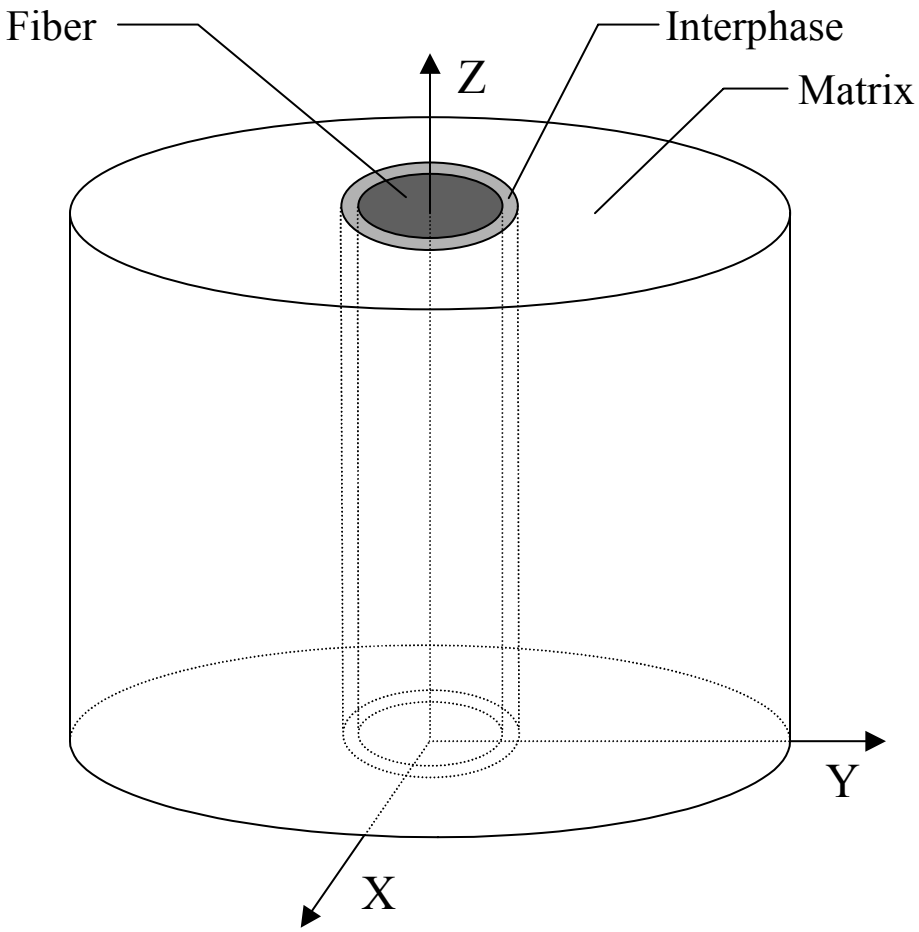

Figure 1a. Schematic model of the unsized carbon fiber configuration

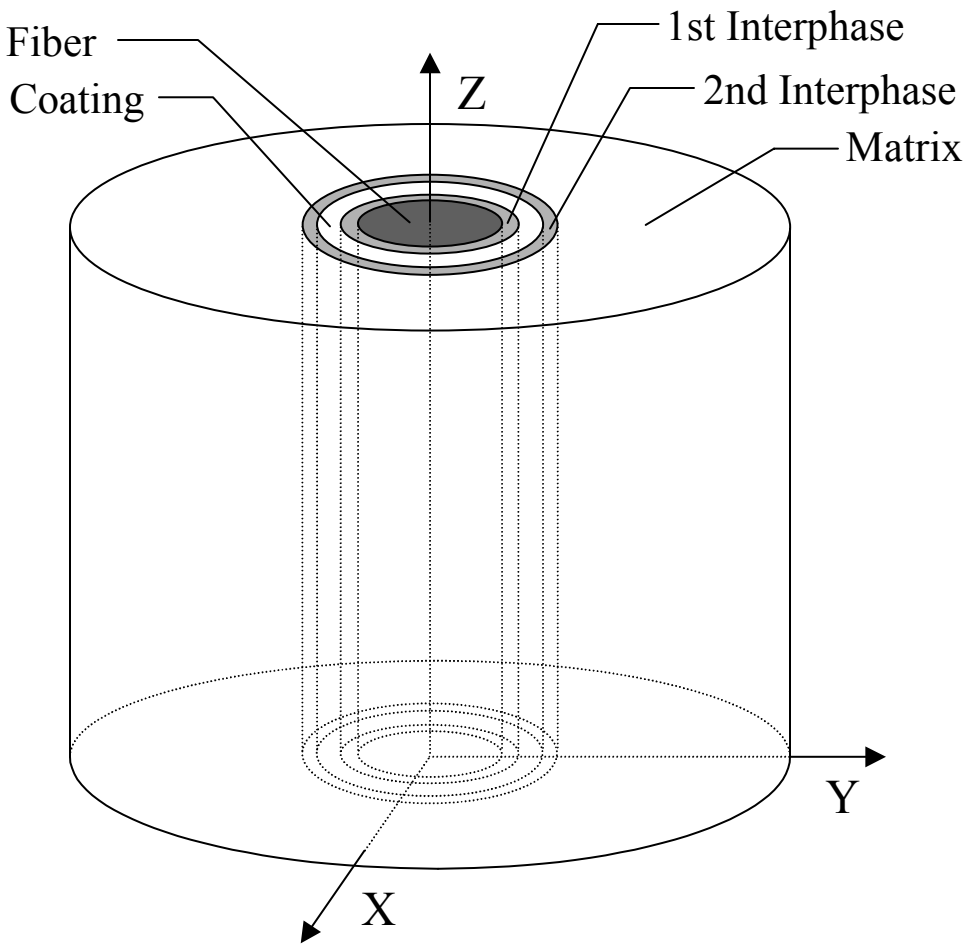

Figure 1b. Schematic model of the coated copper fiber configuration

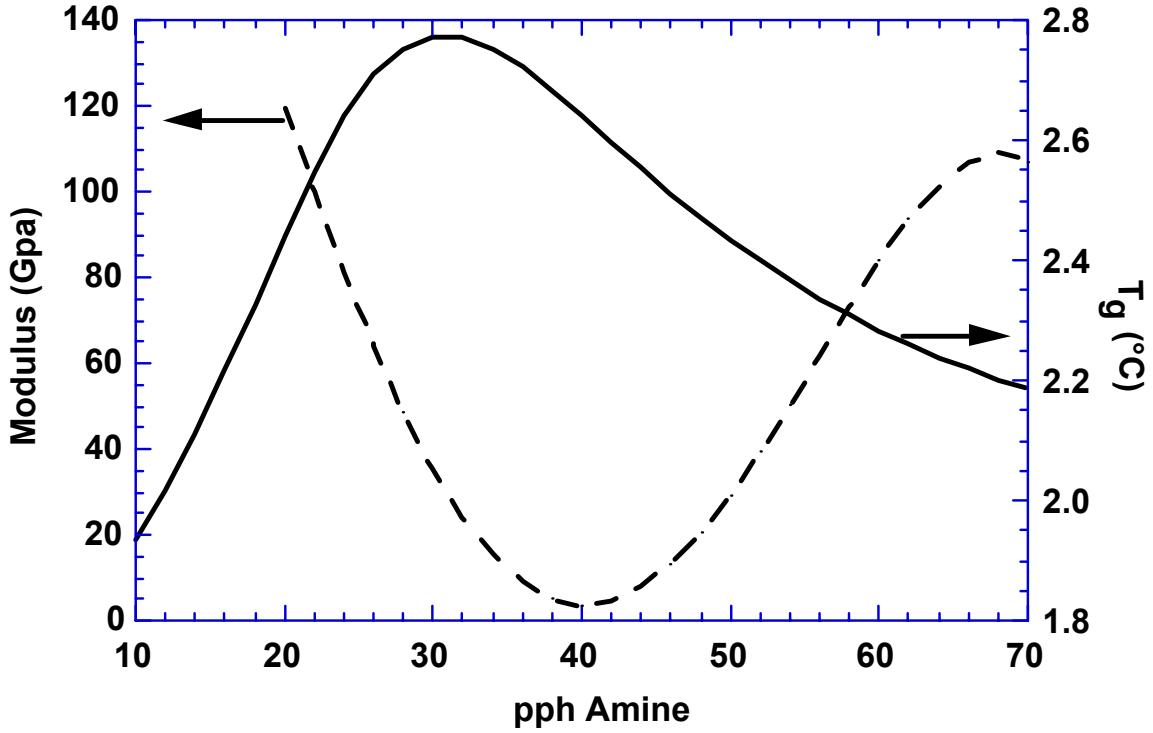

Figure 2. Modulus and T_g dependence on pph amine content

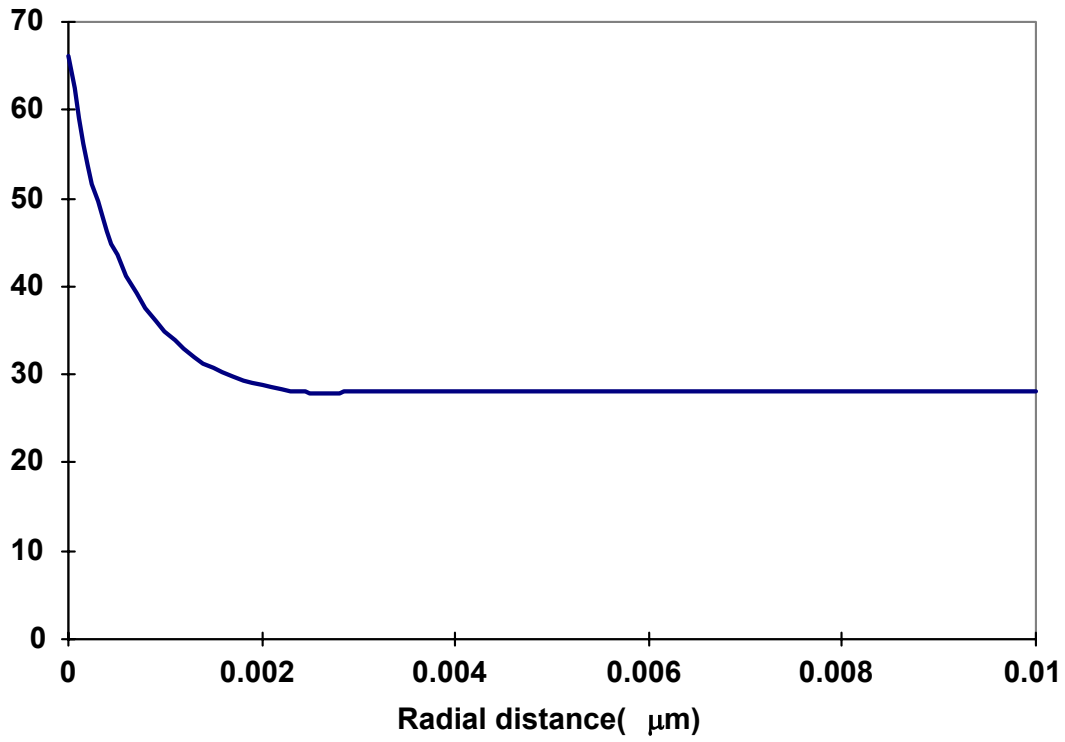

Figure 3. Amine gradient in the interphase of the unsized carbon fiber configuration

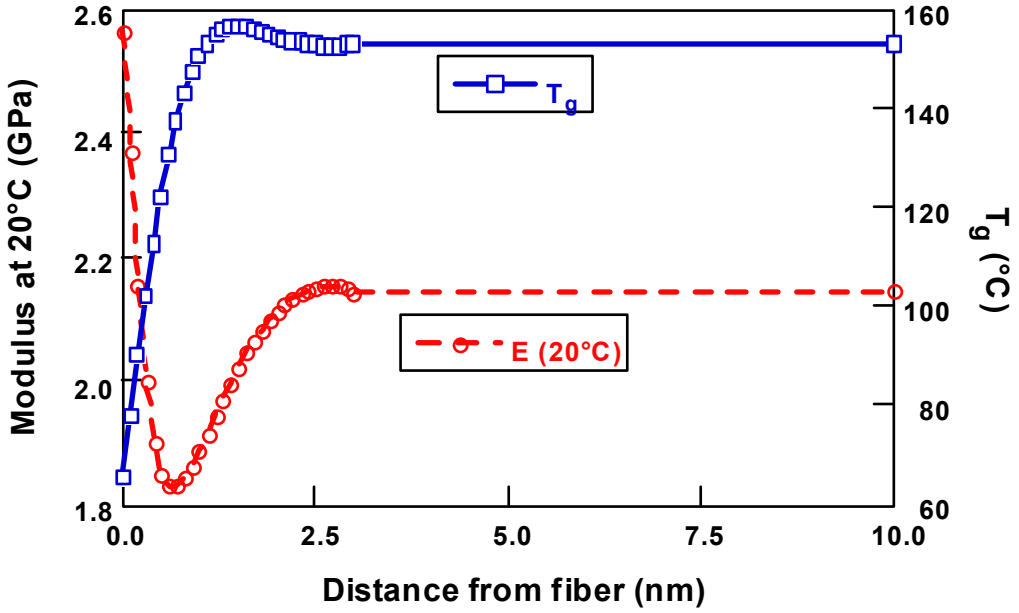

Figure 4. Modulus and T_g gradients in the interphase of the unsized carbon fiber configuration

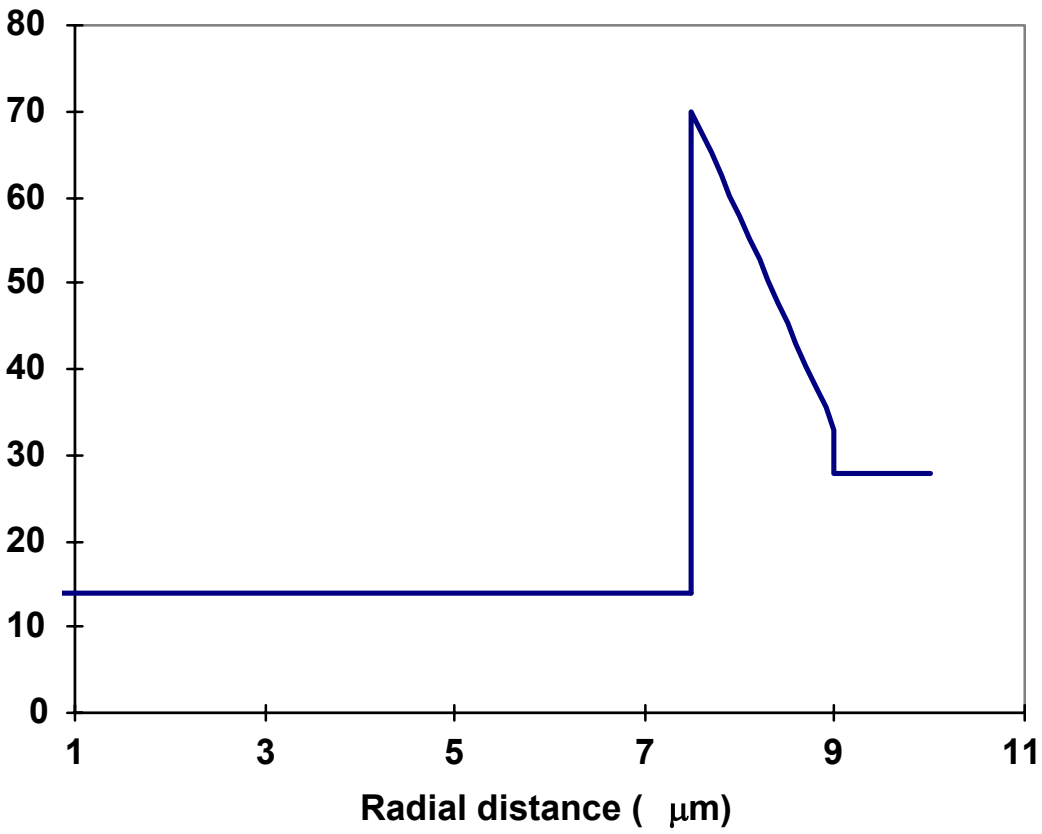

Figure 5. Amine gradient of the coated copper fiber in the coating-matrix interphase region

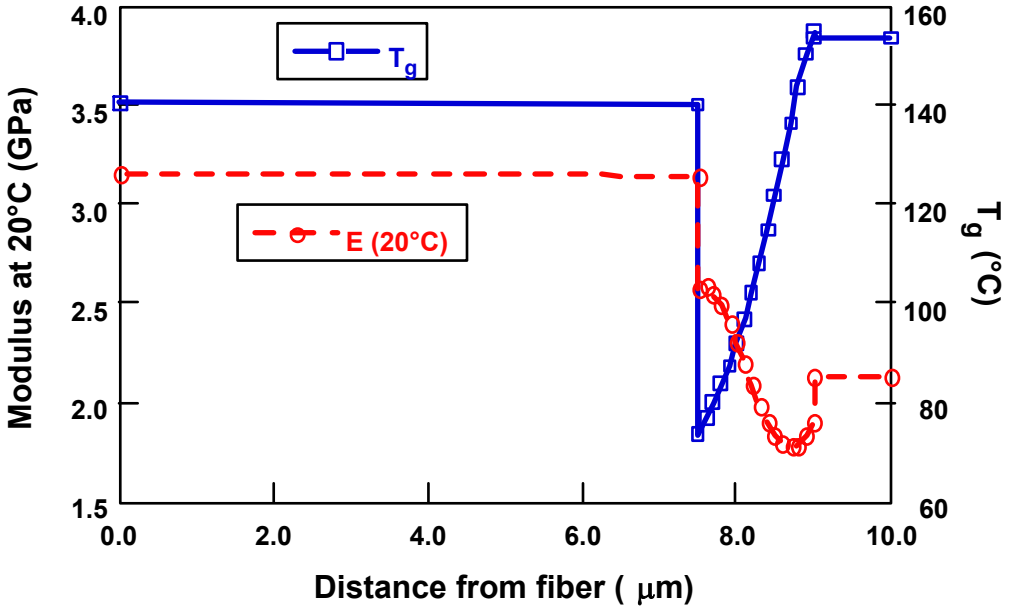

Figure 6. Modulus and T_g gradients in the interphase of the coated copper fiber

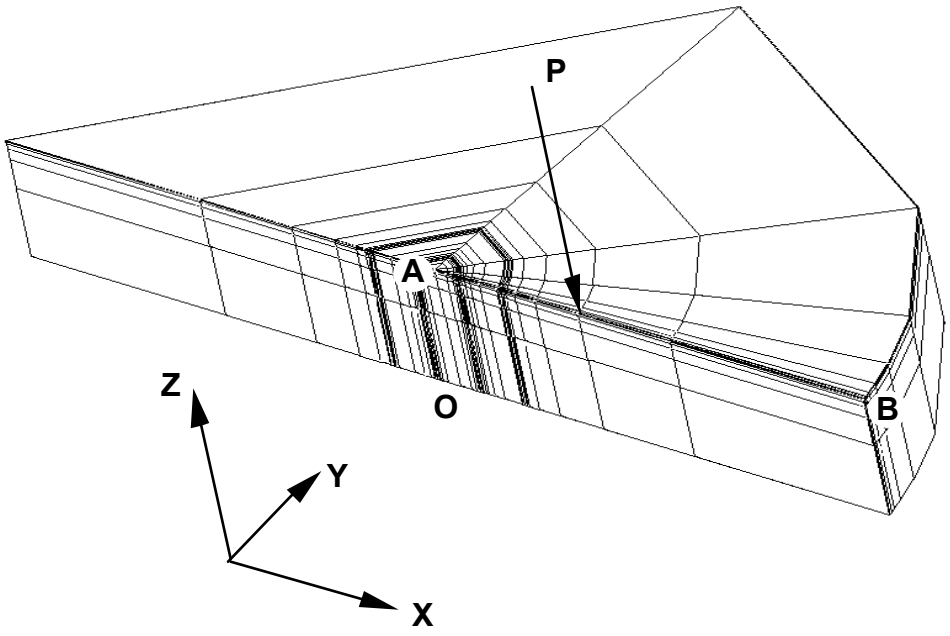

Figure 7. Representative mesh refinement of the finite element model (the coated copper fiber configuration)

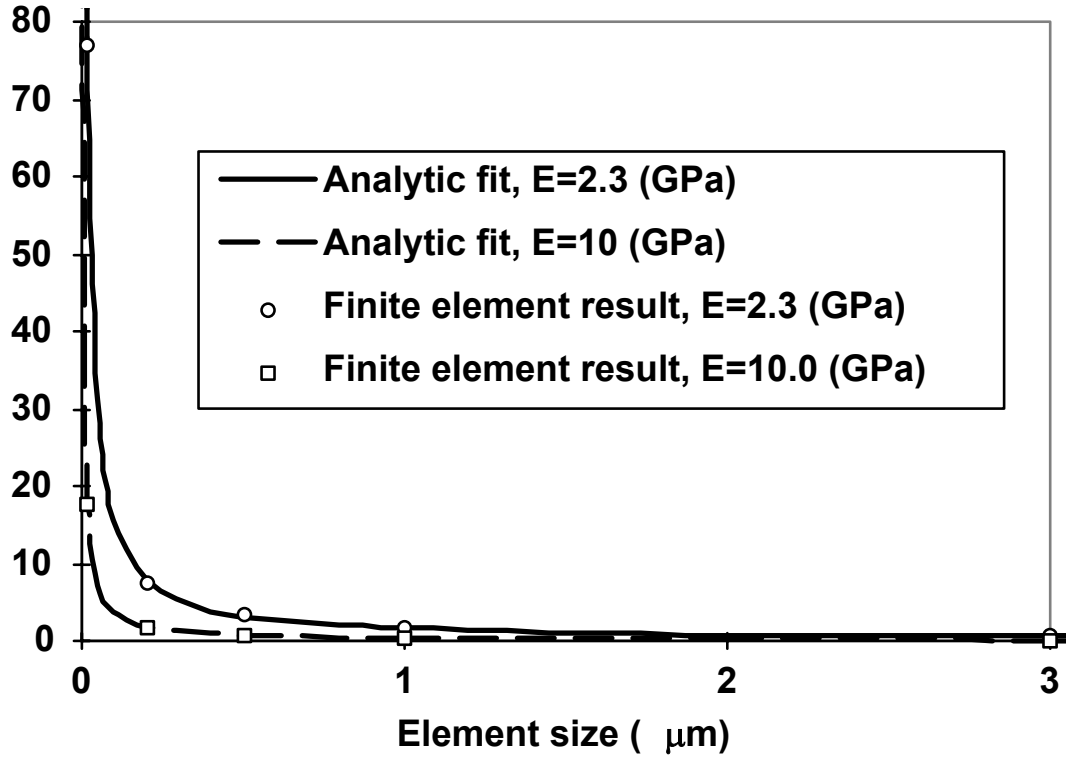

Figure 8. Displacement correlation between analytic fit and numerical results

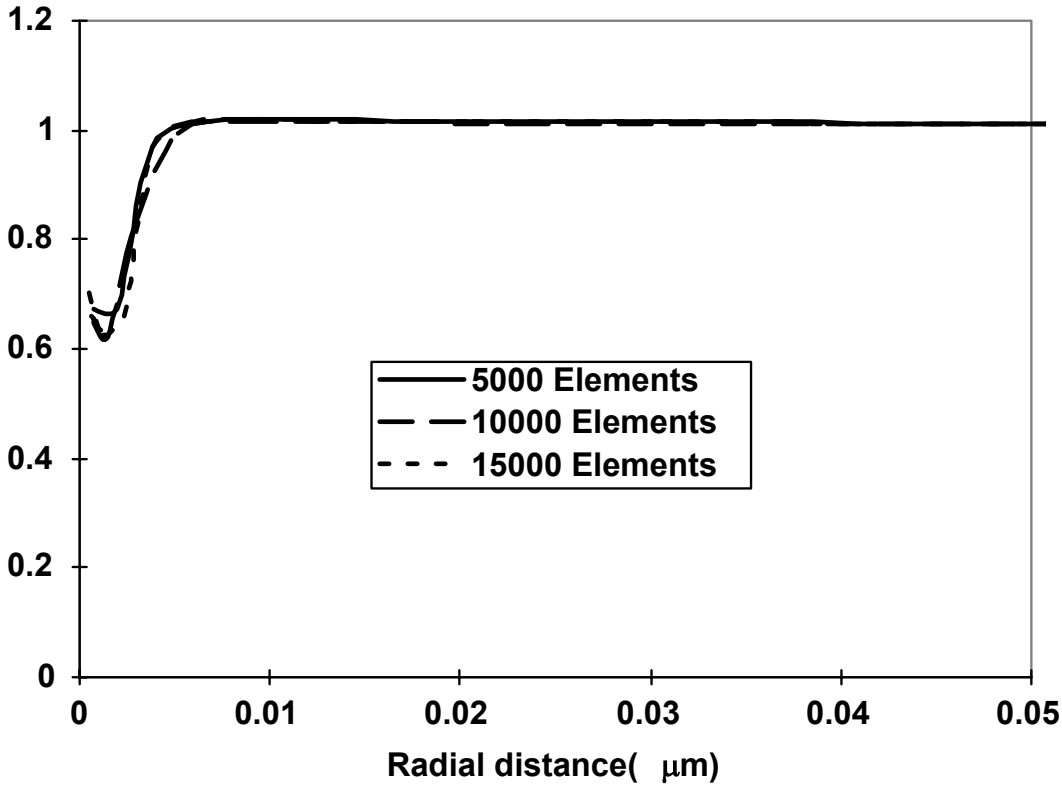

Figure 9. Mesh convergence study for the finite element model

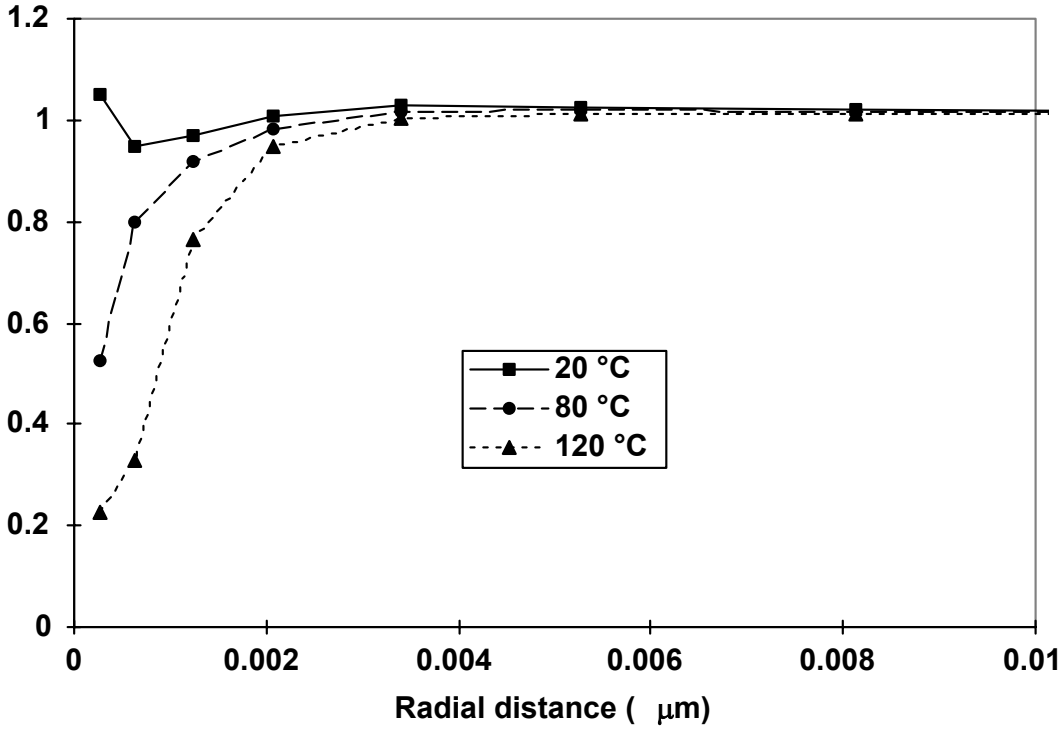

Figure 10. Predicted indentation response of the unsized carbon fiber configuration at 20°C, 80°C, and 120°C

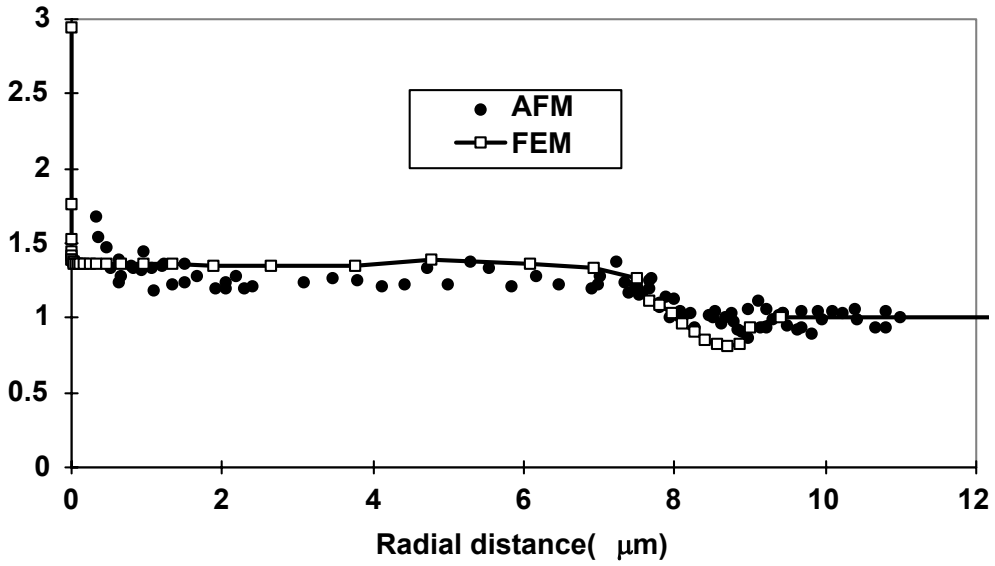

Figure 11. Correlation of the indentation response of the coated copper fiber configuration at 20^{O}C

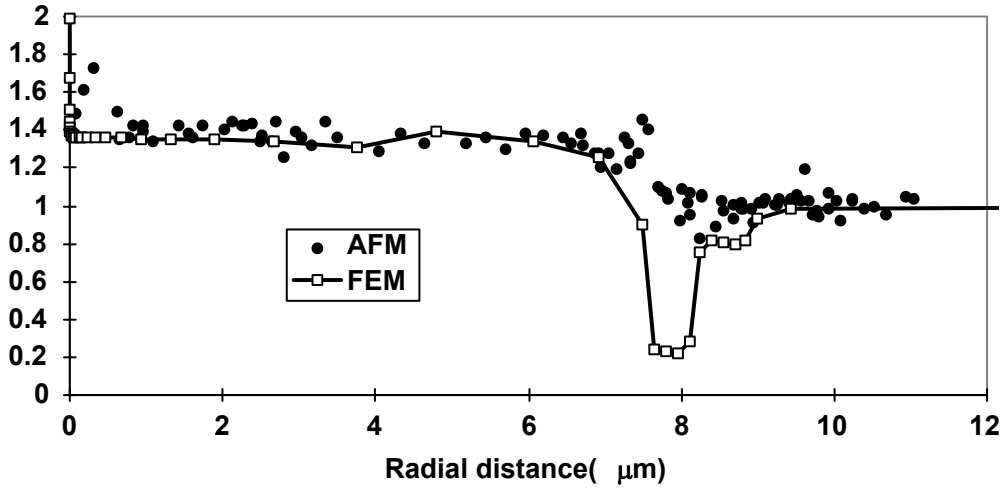

Figure 12. Correlation of the indentation response of the coated copper fiber configuration at 80^{o}C

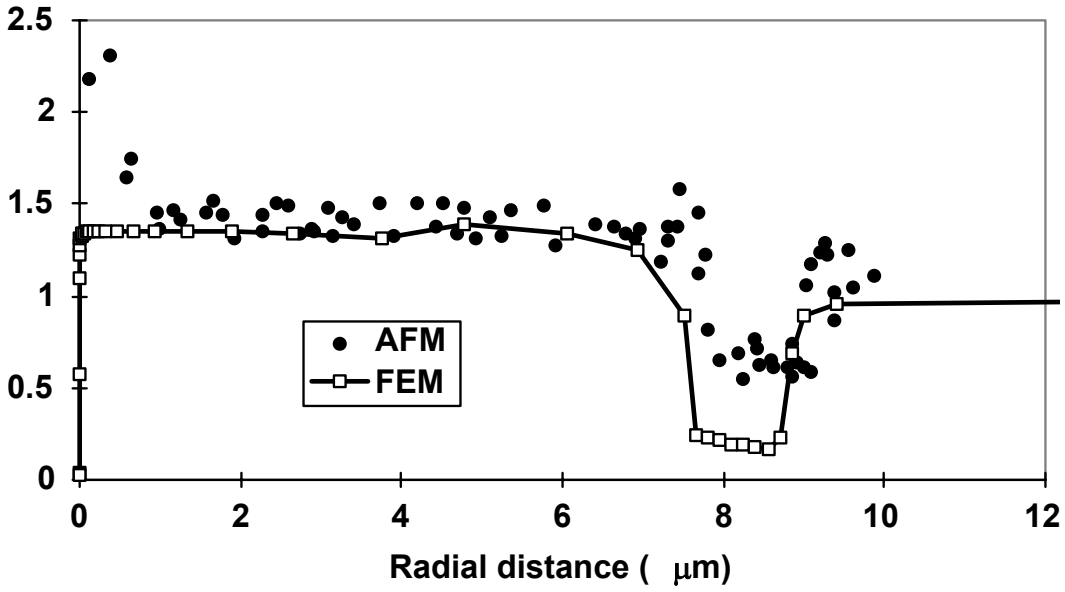

Figure 13. Correlation of the indentation response of the coated copper fiber configuration at 120^{O}C

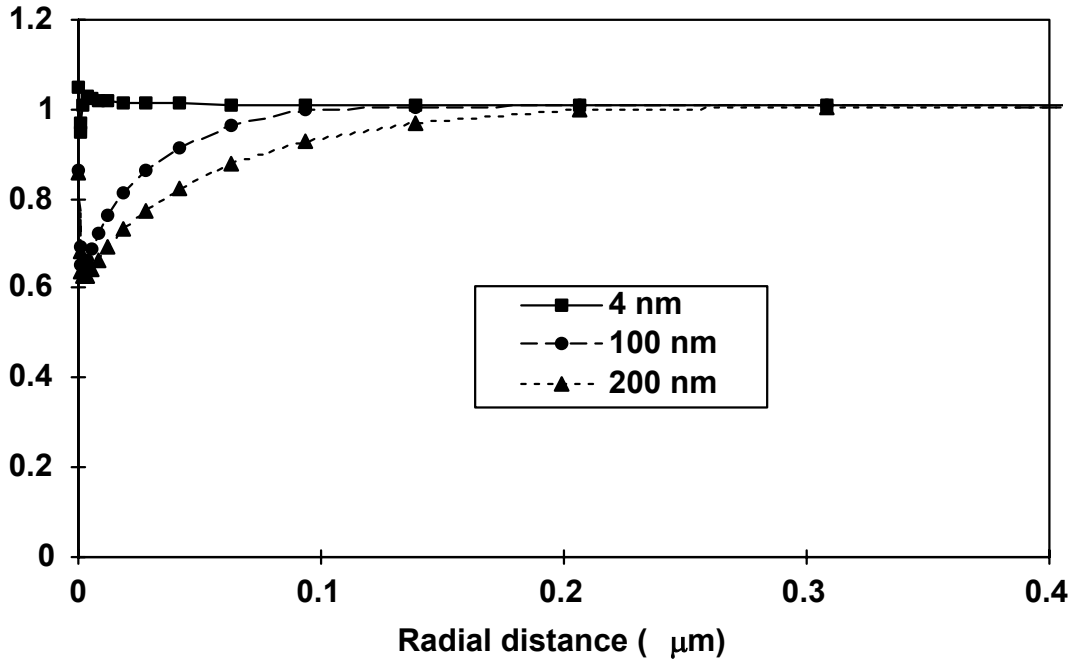

Figure 14. Finite element predictions of the indentation response for various interphase sizes at 20°C

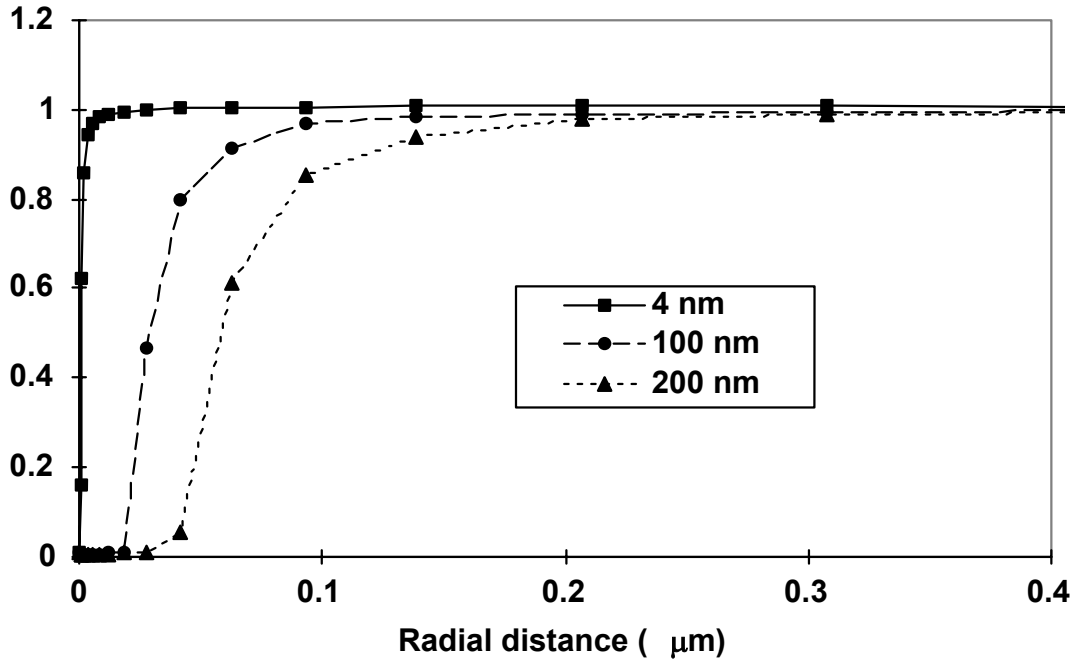

Figure 15. Finite element predictions of the indentation response for various interphase sizes at 120°C